Cognitive Assessment of Scientific Creative-Skill by Brain-Connectivity Analysis Using Graph Convolutional-Interval Type-2 Fuzzy Network

Sayantani Ghosh, *Student Member, IEEE* , Amit Konar, *Senior Member, IEEE* and Atulya K. Nagar

***Abstract*— Scientific creativity refers to natural/automated genesis of innovations in science, propelling scientific, technological, industrial and/or societal progress. Mental paper folding (MPF) requires spatial reasoning, which is an important attribute to determine creative-potential of people. The paper proposes a novel approach to determine creative potential of people from their brain-connectivity network (BCN) during their participation in MPF tasks using functional Near-Infrared Spectroscopy (fNIRS). The work involves three phases. The first phase includes construction of BCN using Pearson's correlation method. The centrality features of the nodes in the network are assessed in the second phase, and transferred to a proposed Graph Convolutional-Interval Type-2 Fuzzy Network (GC-IT2FN) in the third phase to classify the creative potential of individuals in four grades. The novelty of the work includes i) a novel self-attention mechanism in the network to guide graph convolution layers to focus on the most relevant nodes, ii) selection of a new activation function, Logish, after graph convolution to enhance classifier-accuracy, and iii) utilizing the promising region in the Footprint of Uncertainty (FOU) of the used fuzzy sets of IT2FN-based classifier to reduce the effect of uncertainty in brain data on classifier-performance. Experiments conducted demonstrate the efficacy of the proposed framework in contrast to traditional approaches.**

Keywords— scientific creativity, brain connectivity, fNIRS, graph convolution network, interval type-2 fuzzy set.

I. INTRODUCTION

Historically, creativity [1-2] has been intertwined with the domain of art, spanning the origination and realization of a myriad of artistic expressions, from music and painting to poetry, as well as encompassing a broad spectrum of fine arts, culinary pursuits, and performance arts. In contrast, scientific creativity emerges as a distinct facet within the broader conceptual framework of creativity, highlighting its unique focus on unveiling innovation within the scientific domain. Within this context, various cognitive skills play a pivotal role in shaping creative outcomes, such as divergent thinking [3], inductive learning [4], convergent analysis [5], analogical reasoning [6], and the like. Beyond the afore-mentioned cognitive skills, the ability to mentally reshape an object's different attributes (such as shape, orientation, pattern, size etc.) emerges as a pivotal element in the process of creative ideation. This cognitive process, commonly denoted as spatial reasoning [7], has demonstrated its essential role in influencing creative thinking across a spectrum of scientific domains such as mathematics [8-10], engineering [11-12], chemistry [13], medicine [14] etc. The current paper seeks to examine the creative potential of individuals in scientific domain by assessing their spatial reasoning ability through the utilization of functional Near Infrared Spectroscopy (fNIRS).

The spatial reasoning ability of an individual can be evaluated through various cognitive tasks [15], including mental rotation of 2D or 3D figures and mental paper folding (MPF) (which involves visualizing the resulting pattern after a series of folding operations on a piece of paper). The current study focuses on the MPF task to evaluate the spatial reasoning proficiency of subjects. This task involves intricate mental rotations and a sequence of complex visual transformations, thereby providing a comprehensive measure of spatial reasoning [16].

Current literature [17-20] on the MPF task explores the connection between MPF activity and mathematical problem-solving skills. Recently, Dahm *et al*. [21] attempted to investigate the role of action imagery during MPF task. Goumopoulos *et al*., in a very recent study [22], focused on detecting the cognitive load in MPF problem solvers using Electrocardiogram (ECG) signals. In neuroscience studies related to MPF tasks, research predominantly centers on exploring the active regions of the brain during said cognitive activity using functional Magnetic Resonance Imaging (fMRI) [23]-[26], Electroencephalogram (EEG) [27]-[28], or Positron Emission Tomography (PET) scans [16]. There exists hardly any literature on the inter-relationship between creative potential of a subject and his/her brain-connectivity during solving a MPF task. This paper attempts to determine the brain-connectivity involved in a spatial reasoning problem, such as MPF, to assess the creative potential of the subject. In a very recent study, Ghosh *et al*. [29] focused on assessing individuals' creative potential by analyzing EEG signals associated with paper folding skills. Nevertheless, the high cost of brain scanning devices (such as fMRI, MRI, PET, etc.) and the limited spatial resolution of EEG due to volume conductivity [30] preclude their utilization for the current application. In contrast, the fNIRS device provides moderately high spatial resolution at a lower cost and entails minimal computational overhead. Hence, the selection of such a device aligns with the practical considerations for the present application.

The primary aim of the present study is to evaluate the varying levels of creative ability in individuals based on their proficiency in paper folding, employing a classifier built on fNIRS data. This objective is accomplished through a two-stage process. In the initial stage, fNIRS signals collected from subjects engaged in a MPF task are subjected to pre-processing and transformation into a brain connectivity

network (BCN). This network is constructed using the Pearson's Correlation (PC) technique [31]. The selection of the PC technique is motivated by its simplicity, interpretability [32], and demonstrated efficacy across diverse domains [31], [33]-[34]. Following afore-said transformation, the obtained brain networks undergo feature abstraction using three centrality measures (degree, closeness, and betweenness) [35]-[36] to identify the Brodmann Areas (BAs) of the brain that play a central role in coordinating the overall brain network during the MPF based cognitive task. The second stage of the study involves classifying the abstracted features into four distinct degrees of creative potential: High Creative (HCR), Medium Creative (MCR), Low Creative (LCR), and Non-Creative (NCR).

The key contribution of the present research lies in the formulation of a suitable classifier model capable of handling the afore-mentioned classification task. Since the current problem deals with brain connectivity-based features, the classifier is meticulously designed on the principles of a Graph Convolution Network (GCN) [37]-[40], which converts node representations into graph embeddings through the first-order approximation of spectral graph convolutions [37]-[38]. The GCN model comprises two main components where the first part involves an automatic feature learning process using graph convolution and pooling operations, while the second part classifies the pooled vectors using a fully connected (FC) network. However, the fNIRS response acquired from a given source is prone to variations within and across sessions due to undesirable parallel thoughts and various technical and/or physiological artifacts [41]-[42], thereby introducing uncertainty among the pooled feature vectors. To address this issue, the present work introduces a Type-2 Fuzzy Network (T2FN) [43] in conjunction with the GCN. A T2FN adeptly manages the uncertainty among feature vectors by handling intra and inter-session variations [43]-[44]. Consequently, the combined approach of GCN and T2FN aims to enhance classifier performance by mitigating the limitations associated with uncertainties introduced during sessional variations.

In this paper, a novel classifier model, referred to as Graph Convolutional-Interval Type-2 Fuzzy Network (GC-IT2FN) has been designed to categorize individuals with varying spatial problem-solving skills into 4 distinct classes (HCR, MCR, LCR, and NCR) by leveraging the synergies of GCN and T2FN. The novelties of the GC-IT2FN model involves i) introduction of a self-attention mechanism in the GCN that guides the subsequent graph convolution layers to focus on the most significant nodes within the BCN, ii) employment of Logish [45] activation function (due to its inherent negative activation response to signals of small negative amplitude) after the graph convolution operation to enhance the classifier performance, and iii) introduction of a new policy to utilize the most promising region in the Footprint of Uncertainty (FOU) [46]-[47] of the used fuzzy sets of IT2FN to minimize the effect of uncertainty on classifier performance. The policy stated above is accomplished by incorporating a new mapping function to uplift the Lower Membership Function (LMF) of individual type-2 fuzzy sets, thereby utilizing the relatively promising upper region of the FOUs to improve classification accuracy. The efficacy of the proposed GC-IT2FN has been demonstrated through rigorous performance analysis, establishing its superiority over existing state-of-the-art (SOTA) techniques.

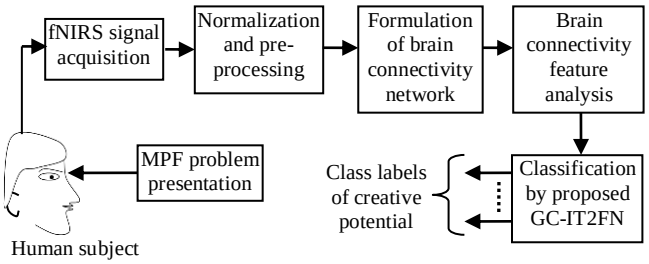

Fig. 1 Schematic overview of the proposed framework

The subsequent sections of the paper encompass the following content. Section II details the principles and methodologies adopted to address the current classification problem. Sections III elaborates the architecture of the proposed classifier and the technique employed to rank individuals based on their creative ability. Section IV presents the experiments and results of the current cognitive experiment. Section V showcases the performance of the proposed classifier in comparison to state-of-the-art techniques. Finally, Section VI offers the inferences drawn from the present work.

II. Proposed Framework

This section provides a concise overview of the experimental paradigm, with Fig. 1 illustrating the schematic diagram of the entire system. The experiment initiates by capturing fNIRS signals from the participants' scalp during their engagement in the MPF task. The visual stimuli structure for the current application pertaining to a single session is depicted by Fig. 2. A single session comprises 5 trials where each trial begins by 3-second presentation of a fixation cross. Subsequently, a 15-second time-window follows, presenting the mental problem that participants are required to solve. For the present application, the MPF task involves participants to view diagrams depicting the folding of a paper and the punching of a hole (of any shape) within it. The challenge then prompts participants to mentally envision the spatial arrangement of the holes after unfolding the paper [48]-[49]. An example of such a problem is illustrated in Fig. 3. After this phase, the visual stimuli consist of a 30-second time-window during which participants communicate their answers to the experimenter by drawing their attempted solution to the MPF task on a sheet of paper. The afore-mentioned process is repeated for 20 different problem sets within a single trial. Notably, a 30-second time gap is preserved between consecutive trials to alleviate the potential residual effect of the preceding stimulus. The entire experiment is composed of 5 sessions, each encompassing 5 trials. Across 10 experimental days, a total of 5000 experimental instances per subject are generated for the present scenario, calculated as follows: 20 problems/trial × 5 trials/session × 5 sessions/day × 10 days.

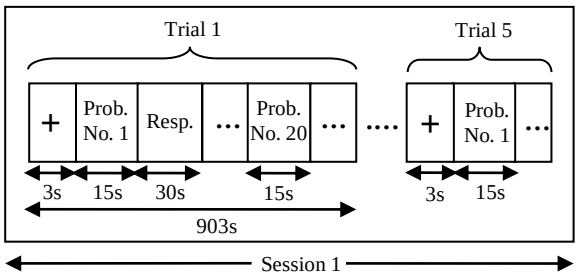

Fig.2. Visual stimuli utilized for a single session of the MPF task

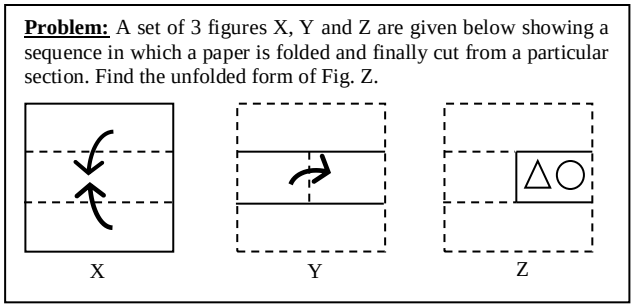

Fig. 3. Exemplar problem utilized for the MPF task

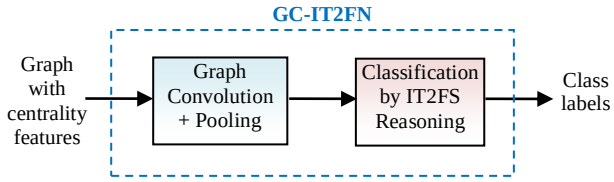

Fig. 4. Architectural overview of the proposed GC-IT2FN model

The fNIRS signals acquired from the acquisition phase undergo normalization, pre-processing, and transformation into a brain connectivity network for an in-depth analysis of inter-lobe interactions during the ongoing cognitive task. Subsequently, brain connectivity based centrality features are derived and employed as input to a novel GC-IT2FS classifier, designed to categorize subjects' creative abilities into 4 distinct classes.

The 4 categories of class labels (HCR, MCR, LCR, NCR) were determined based on a scoring policy framed by 10 spatial reasoning experts. Here, each paper folding task involves 3 steps of folding and a run-through punching of the paper, where the results of unfolding the 4 segments of the paper is independent of the order of folding the paper. After a detailed discussion among the experts, a consensus about the following scoring policy was decided. For each segment of a paper-folding task, 25 marks are assigned. Again, within each segment, 5 points are reserved for correctly identifying number and type (e.g., circular/triangular) of cuts, 8 points for correctly identifying the order of type of cuts (e.g., circle followed by triangle in left-to-right order), and 12 marks for correctly identifying the orientation of the shaped cuts (e.g., inverted/upright triangles). The sub-score for each segment of a paper is evaluated first by adding the scores for above 3 items and the final score out of 100 is the sum of the sub-totals for four segments of a paper. A few samples of solutions provided by the subjects and their corresponding scores have been included in Section A.3 of the Appendix [93].

The detailed procedures involved in the present classification task are elucidated below.

A. Normalization of Raw fNIRS data

The raw fNIRS signals acquired from the scalp of subjects consists of two types of blood concentrations: oxy-hemoglobin blood concentration (in mmol/L) and deoxy-hemoglobin blood concentration (in mmol/L). Let the oxy-hemoglobin blood concentration and deoxy-hemoglobin blood concentration for the λ^{th} channel corresponding to a given montage during a time-interval τ be denoted as $CHbO(\tau)$ and $CHbR(\tau)$ respectively. Since, $CHbR(\tau) < CHbO(\tau)$ for all τ from a brain region corresponding to the given montage [44], the normalization of fNIRS signals is performed by first computing (1) and (2).

$$Max(CHbO) = Max_{\tau}(CHbO(\tau) : \tau_s \le \tau \le \tau_e, \forall\lambda) \quad (1)$$

$$Min(CHbR) = Min_{\tau}(CHbR(\tau) : \tau_s \le \tau \le \tau_e, \forall\lambda) \quad (2)$$

where, τ_s and τ_e represent the starting and ending time of an experimental trial respectively corresponding to a given stimuli for a particular subject. Next, in order to evaluate the oxygen consumption during a time instant τ, the difference between the values of oxy-hemoglobin and deoxy-hemoglobin blood concentration is considered. The afore-said evaluation is represented by (3).

$$d(\tau) = CHbO(\tau) - CHbR(\tau) \quad (3)$$

The normalized value of the difference signal in (3) within the range of [0,1] during a time instant τ is computed using (4).

$$\hat{d}(\tau) = \frac{CHbO(\tau) - CHbR(\tau)}{Max(CHbO) - Min(CHbR)} \quad (4)$$

B. Pre-Processing Stage

The data acquired from a fNIRS device, like any measurement method, it is susceptible to various forms of artifacts. The prevalent types of artifacts that deserve special consideration are: i) physiological artifacts and ii) technical artifacts [41]-[42]. Physiological artifacts are related to biological processes within the human body and can be categorized into 3 main classes [41], [50]-[52]: a) Motion Artifacts: they are caused by head movements, muscle contractions, or other bodily motions, b) Systemic Physiological Artifacts: they arise due to the fluctuations in blood pressure, heart rate, and respiration and c) Skin Blood Flow Artifacts: they occur due to changes in blood flow within the skin, such as those related to skin temperature and emotional responses like blushing. Technical artifacts in fNIRS signals are related to different aspects of instrumentation, data acquisition, and the environment in which the measurements are taken. In other words, they arise due to fluctuations in light intensity, interference from other nearby electrical devices, optode placement instability etc. [42].

To eliminate the afore-mentioned artifacts from the raw fNIRS signal, a rigorous signal processing approach is

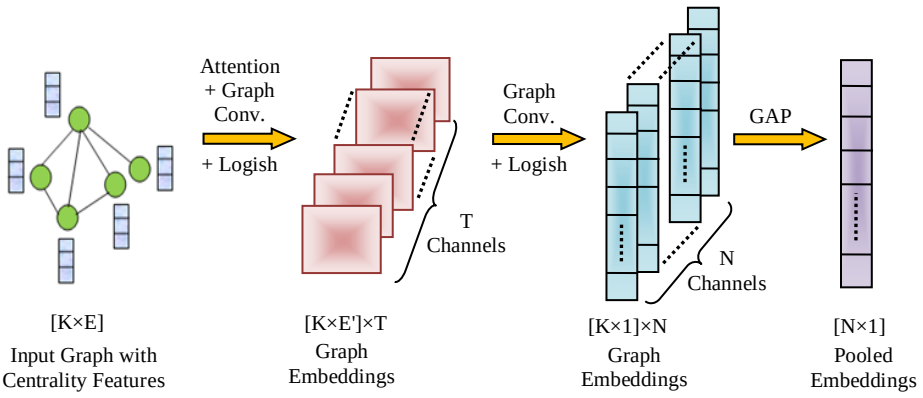

Fig. 5. Formation of global average pooled embeddings

employed. Initially, the normalized difference signal $\hat{d}(\tau)$ for $\lambda = 1$ to H channels undergoes filtering using an Elliptical band-pass filter of order 4, with a pass band range set at 0.1-2 Hz. The selection of the Elliptical band-pass filter is made due to its sharp roll-off characteristics around the cut-off frequency, ensuring precise isolation of the desired frequency components while effectively attenuating noise and artifacts [53]. Subsequent to the filtering stage, Independent Component Analysis (ICA) [54] is applied to the filtered signals. This technique helps to restore the independent hemodynamic components corresponding to each channel.

C. Formulation of Brain Connectivity Network (BCN)

In this sub-section, the pre-processed fNIRS signals are transformed into a connectivity graph to explore the interaction between the different BAs involved in the current cognitive task. The afore-said exploration begins by computing the Pearson's correlation coefficient for every pair of fNIRS channel using (5).

$$\rho_{XY} = \frac{1}{h-1}\sum_{i=1}^{h}\left(\frac{x_i - \bar{x}}{\sigma_X}\right)\left(\frac{y_i - \bar{y}}{\sigma_Y}\right) \tag{5}$$

In (5), ρ_{XY} represents the correlation coefficients values for a pair of fNIRS channels X and Y, h represents the number of data points pertaining to a given fNIRS channel, $\bar{x}, \bar{y}, \sigma_X$ and σ_Y represent the mean and standard deviation values of the data points of fNIRS channels X and Y respectively.

The above computation yields a $K \times K$ matrix representing the correlation between a pair of fNIRS channels. In the next step, the correlation coefficients are normalized using max-min normalization technique [55]. The normalized coefficients are utilized to construct an undirected (binary) graph or BCN by adopting the following strategy.

$$\alpha_{ij} = \begin{cases} 1, & if\ \hat{\rho}_{ij} \geq \zeta \\ 0, & otherwise \end{cases} \tag{6}$$

where α_{ij} represents the adjacency matrix values of the graph, $\hat{\rho}_{ij}$ denotes the normalized Pearson's correlation coefficients and ζ indicates a pre-defined threshold. The pre-defined threshold has been carefully chosen to ensure that all the connectivity networks/graphs share the same mean degree, facilitating their straight-forward comparability [56].

D. Feature Extraction of Brain Connectivity Network

The brain connectivity networks acquired using PC technique needs to be quantified to explore the hub nodes controlling the entire brain network. The afore-mentioned quantification is performed by abstracting three features: degree centrality (DC), closeness centrality (CC) and betweenness centrality (BC) [35]-[36].

The abstracted features are ultimately classified into four distinct classes using the GC-IT2FN classifier, the intricate architecture of which is thoroughly explained in the following section.

III. Proposed Graph Convolutional-Interval Type-2 Fuzzy Network (GC-IT2FN)

The architectural overview of the proposed GC-IT2FN model is illustrated in Fig. 4 which comprises two main modules: i) a graph convolutional block and ii) IT2FS classifier. The functionality of each layer is elucidated below.

A. Attention Induced First Graph Convolution Layer with Logish Activation Function

The initial layer of the proposed model involves two primary operations: an attention-induced graph convolution operation and the application of the Logish activation function. The detailed aspects of the aforementioned operations are discussed below and illustrated in Fig. 5.

A.1. Attention Induced Graph Convolution

The traditional graph convolution operation [37] abstracts the necessary features from the input graph $P \in \Re^{K \times E}$ and transforms it into low dimensional vectors of size $K \times E'$ (where, $E' < E$) or graph embeddings using (7).

$$Z_j^{l+1} = \sigma\left(\sum_i \hat{A} Z_i^l W_{ij}^l\right) \tag{7}$$

where, $Z^l \in \Re^{K\times E}$ denotes the input graph in the l^{th} layer and $Z^0 = P$. $\hat{A} = \tilde{D}^{-1/2}\tilde{A}\tilde{D}^{-1/2}$ represents the normalized graph Laplacian [37] that consists of the structural information inherent in the graph. $\tilde{A} = A + I$ indicates the adjacency matrix comprising self-loops while $I \in \Re^{K\times K}$ signifies the identity matrix. $\tilde{D} = D + I$, where D represents the diagonal degree matrix and $\tilde{D}_{i,i} = \sum_j \tilde{A}_{ij}$. W_{ij}^l denotes the input to hidden layer trainable weight matrix. $\sigma(\cdot)$ signifies an activation function that adds non-linearity within the given neural network.

However, the present work introduces a self-attention mechanism before graph convolution operation that helps the subsequent graph convolution layers to focus on the most relevant nodes. Such a self-attention mechanism computes the attention coefficients between adjacent nodes *i* and *j* with feature vectors p_i and p_j using (8).

$$\phi_{ij} = \frac{1}{\exp(\| p_i - p_j \|_1)} \tag{8}$$

where, ϕ_{ij} denotes the attention coefficients between adjacent nodes *i* and *j* while $\|\cdot\|_1$ represents the L1 norm operation. In (8), the L1 norm operation assesses the similarity or proximity of feature vectors for two nodes. Consequently, a lower L1 norm value suggests greater similarity between nodes, while a higher value indicates dissimilarity. Nevertheless, to assign greater attention weights to similar nodes, the reciprocal of the L1 norm operation is considered. Furthermore, in (8), the result of the L1 norm undergoes an exponential operation prior to the afore-said reciprocal operation. This process ensures that the attention coefficient for the self-node ϕ_{ii} attains the maximum attention value i.e., 1, while attention coefficients among other nodes ϕ_{ij} are confined within the range (0, 1). For the current scenario, if a node m is not a neighbor of node i, then (8) is not applicable and thus $\phi_{im} = 0$ is considered.

The attention coefficient values for node *i* with respect to all the nodes within the graph forms a coefficient vector $\vec{\phi}_i = [\phi_{i1}, \phi_{i2}, ..., \phi_{iK}]^T$. The coefficient vectors for all the nodes within the graph collectively constitute a $K \times K$ matrix $\Phi = [\vec{\phi}_1, \vec{\phi}_2, ..., \vec{\phi}_K]$ which is symmetric i.e., $\phi_{ij} = \phi_{ji}$.

In order to make the graph convolution layers focus on the most important nodes, the matrix Φ is utilized to modify the graph Laplacian using (9).

$$\hat{M} = \hat{A} \otimes \Phi \tag{9}$$

where, $\hat{M}$ represents the modified graph Laplacian and $\otimes$ denotes the Hadamard product. After this, the modified graph Laplacian is employed in the graph convolution operation as shown in (10).

$$Z_j^{l+1} = \sigma(\sum_i \hat{M} Z_i^l W_{ij}^l) \tag{10}$$

Thus, the modified Laplacian matrix enables the convolution layers to concentrate on specific aspects of the graph structure. This, in turn, serves as a mechanism to enhance the encoding of the underlying relationships and patterns within the graph.

A.2. Utilization of Logish Activation Function

Although various conventional activation functions could have been employed to introduce non-linearity to the classifier, the authors have specifically chosen to use the Logish [45] activation function for the current scenario. This particular activation function is preferred for several reasons. Its non-linear nature ensures that the neural network does not reduce to a mere linear operation, enhancing its capacity to capture complex patterns in the data. Another distinctive feature of Logish is its unbounded nature above, effectively addressing

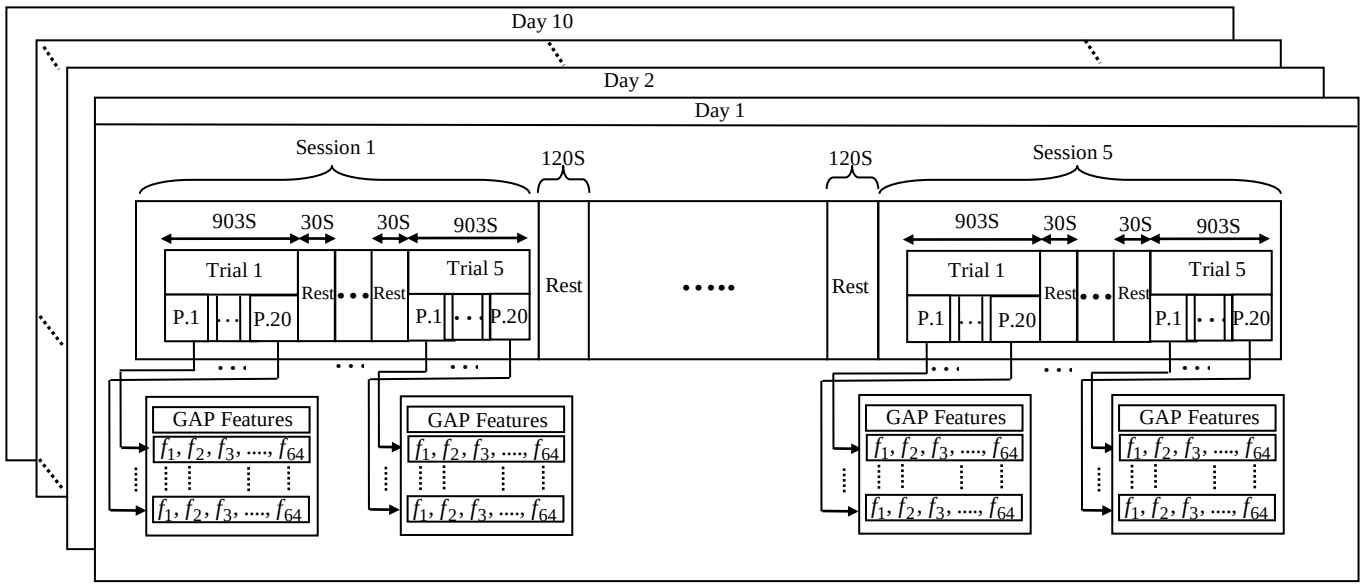

Fig. 6. The GAP features acquired from 5 sessions, each containing 5 trials (every trial containing 20 MPF problems), repeated over 10 experimental days.

the vanishing gradient problem and promoting a faster convergence rate for the classifier. Furthermore, the activation function is bounded below, contributing to a robust regularization effect that aids in preventing over-fitting. Additionally, the non-monotonic behavior of the Logish function (i.e., imparting small negative magnitude for small negative input value) plays a crucial role in stabilizing the training of negative values, thereby increasing the overall stability of the network. This unique set of properties associated with the Logish activation function serves as a strong motivation for its utilization in the current application, enhancing the expressive capabilities of the neural network while addressing common challenges in training and convergence. The mathematical expression of Logish is indicated by (11).

$$\sigma(x) = Logish(x) = x \cdot \ln(1 + sigmoid(x)) \tag{11}$$

B. Second Graph Convolution Layer with Logish Activation Function

To capture higher-level features, another graph convolution operation (as shown in Fig. 5) is applied to the convolved output from the initial layer using equations (7) and (11). This strategic choice enables the network to extract and learn more complex features, enhancing its capability to understand intricate patterns within the data [57].

C. Global Average Pooling Layer

Global average pooling (GAP) is a pooling operation that reduces the spatial dimensions of a feature map to a single value per feature channel by taking the average of all values in that channel [57]. Let $\vec{V} \in \Re^{K\times 1\times N}$ be the feature map that has been computed by the second graph convolution operation where $K\times 1$ denotes the size of each feature map while N represents the number of feature channels. Let the i^{th} feature vector of $\vec{V}$ having size $K\times 1$ be denoted as $\vec{V_i} = [v_1, v_2, ..., v_K]^T$. The GAP operation for $\vec{V_i}$ is represented by (12).

$$\beta(\vec{V_i}) = (v_1 + v_2 + ... + v_K)/K \tag{12}$$

where, $\beta(\cdot)$ represents the GAP function.

D. Interval Type-2 Fuzzy layer

The GAP operation produces a feature vector of size $N\times 1$ (where $N = 64$) for every MPF problem as shown in Fig. 6.

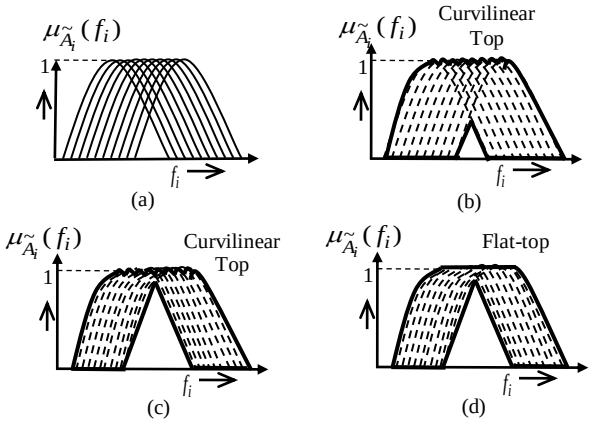

Fig.7. Formulation of IT2FS with modified FOU (a) Type-1 MFs for 10 days (b) Curvilinear-top based IT2FS produced by union of Type-1 MFs (c) Curvilinear-top based IT2FS with modified FOU (d) IT2FS with flat-top approximation

The management of uncertainty introduced within these GAP vectors due to sessional variations is accomplished through an Interval Type-2 Fuzzy Network (IT2FN), the details of which are elaborated below.

D.1. Antecedent Construction of IT2FS

Let, $f_1, f_2, ..., f_N$ be N number of features acquired after the GAP operation. Let $\tilde{A}_i$ for i=1 to N represent an IT2FS defined as $[\overline{\mu}_{\tilde{A}_i}, \underline{\mu}_{\tilde{A}_i}]$ for a given linguistic variable f_i as the upper and lower membership function of $\tilde{A}_i$. For the present scenario, $\tilde{A}_i$ has been constructed considering both inter-session (5 sessions in an experimental day) as well as intra-session (5 trials within a session) variations in f_i (representing one average pooled feature). For the afore-said formulation, the initial step involves constructing one Type-1 Gaussian MF by determining the mean (m) and variance (σ^2) among all the f_i values obtained in an experimental day as illustrated in Section A.1. of the Appendix [93]. The constructed Gaussian MF has the center of the base positioned at m and the two extremities situated at $m \pm 3\times\sigma$ [58]. Since the experiment has been conducted for 10 days, 10 such Type-1 Gaussian MFs are obtained, and these are utilized for the construction of IT2FS, as depicted in Fig. 7(a).

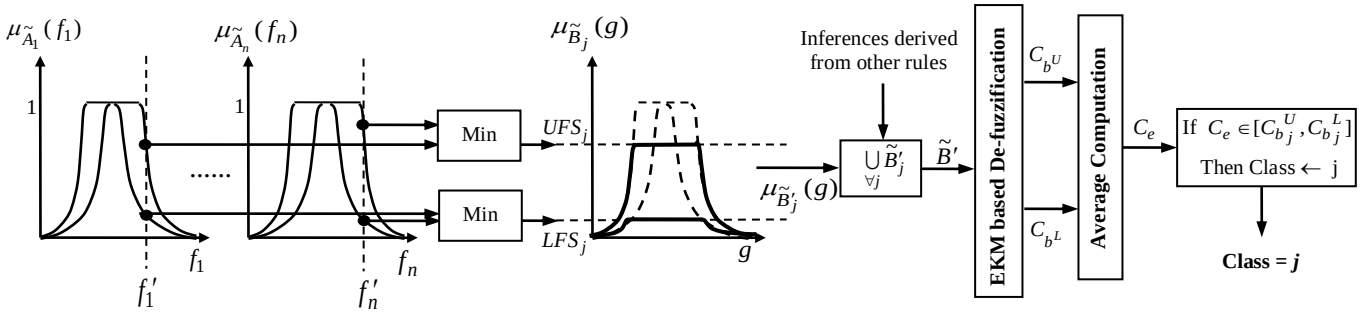

Fig. 8. The formulation of IT2FN classifier

Fig. 9. Subject participating in the MPF based cognitive task

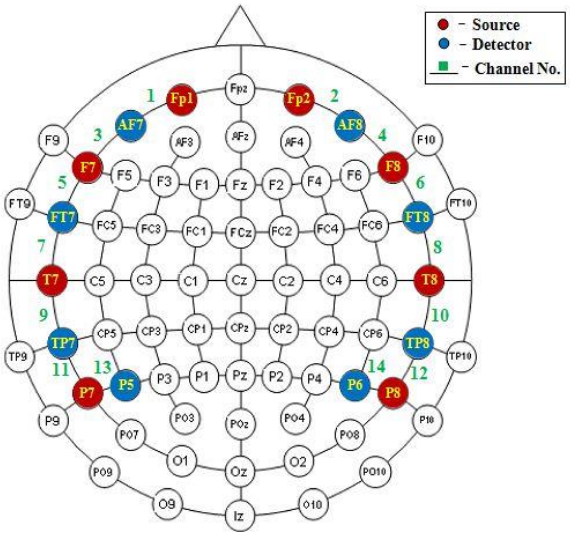

Fig. 10. Montage utilized for the MPF task

An interval type-2 membership function (IT2MF) $\tilde{A}_i$ is developed by computing the union of 10 Type-1 MFs as depicted in Fig. 7(b). The UMF and LMF of $\tilde{A}_i$ is constructed by employing the mathematical operations denoted by (13-14).

$$UMF = \bar{\mu}_{\tilde{A}_i}(f_i) = \max(\mu_{\tilde{A}_1}(f_1), \mu_{\tilde{A}_2}(f_2), ..., \mu_{\tilde{A}_N}(f_N)) \quad (13)$$

$$LMF = \underline{\mu}_{\tilde{A}_i}(f_i) = \min(\mu_{\tilde{A}_1}(f_1), \mu_{\tilde{A}_2}(f_2), ..., \mu_{\tilde{A}_N}(f_N)) \quad (14)$$

However, the promising contribution of embedded T1-fuzzy sets to the FOU lies in the local neighborhood region of the UMF inside the FOU. To utilize this promising region of the FOU, a mapping function is introduced to level up the LMF towards the UMF, thereby reducing the area under the modified FOU as depicted in Fig. 7(c). The mapping function for constructing the refined LMF is denoted by (15).

$$LMF_{\mathrm{Re}} = \underline{\mu}_{\tilde{A}_i'}(f_i) = \left(\bar{\mu}_{\tilde{A}_i}(f_i)^{\exp(\underline{\mu}_{\tilde{A}_i}(f_i))} \right)^{\eta} \quad (15)$$

where, $\eta \geq 1$ indicates a hyper-parameter that is fine-tuned during the training process. The term $\bar{\mu}_{\tilde{A}_i}(f_i)^{\exp(\underline{\mu}_{\tilde{A}_i}(f_i))}$ in equation (15) reduces the area under the FOU, with η acting as a reduction ratio. In other words, the term $\bar{\mu}_{\tilde{A}_i}(f_i)^{\exp(\underline{\mu}_{\tilde{A}_i}(f_i))}$ functions to decrease the area under FOU while the hyper-parameter η governs the extent of this reduction. Thus, by adjusting η, the classifier can control the effective management of variations within and across sessions to achieve improved performance. The UMF of the modified FOU remains same as (13) i.e., $\bar{\mu}_{\tilde{A}_i'}(f_i) = \bar{\mu}_{\tilde{A}_i}(f_i)$. It can be verified from (15) that $\underline{\mu}_{\tilde{A}_i'}(f_i) \leq \bar{\mu}_{\tilde{A}_i'}(f_i)$, for all f_i.

However, during the computation of the UMF for IT2FS, a curvilinear top is generated by taking the maximum of the 10 Type-1 MFs, as illustrated in Fig. 7(b) and (c). To ensure the convexity of the constructed Type-2 fuzzy sets, a flat-top approximation is applied to the obtained IT2FS. This process involves connecting the peaks of the individual Type-1 MFs with a straight line characterized by a zero slope [4], [43]. The resulting flat-top approximated IT2FS is depicted in Fig. 7(d).

D.2. Classifier Rule

The classifcation rule R_j is presented below.

If f_1 *is* $\tilde{A}_1'$, *and* f_2 *is* $\tilde{A}_2'$ *and...and* f_N *is* $\tilde{A}_N'$, *Then* g *is* $\tilde{B}_j$ *lying in* $[C_{b_j^U}, C_{b_j^L}]$. Here, $\tilde{B}_j$ denotes the consequent MF of the j^{th} interval type-2 fuzzy class having class centroid within upper and lower class boundary $C_{b_j^U}$ and $C_{b_j^L}$ respectively. The consequent MF $\tilde{B}_j$ is formulated based on the intra-session and inter-sesssion variations of the scores assigned to each written response as discussed in Section II. The subsequent steps in the IT2FS construction for the consequent part follow the same process as outlined for the antecedent part in the preceding sub-subsection *D.*1.

D.3. Design of IT2FS Classifier

The architecture of the IT2FS based classifier is demonstrated in Fig.8. Let the measurements points be $f_1 = f_1', f_2 = f_2', ..., f_N = f_N'$. The Upper Firing Strength (UFS) and Lower Firing Strength (LFS) of rule j is evaluated by (16) and (17) respectively.

$$UFS_j = \min[\bar{\mu}_{\tilde{A}_1'}(f_1'), \bar{\mu}_{\tilde{A}_2'}(f_2'), ..., \bar{\mu}_{\tilde{A}_n'}(f_N')] \quad (16)$$

$$LFS_j = \min[\underline{\mu}_{\tilde{A}_1'}(f_1'), \underline{\mu}_{\tilde{A}_2'}(f_2'), ..., \underline{\mu}_{\tilde{A}_n'}(f_N')] \quad (17)$$

Now, the IT2 inference $[\bar{\mu}_{\tilde{B}_j'}(g), \underline{\mu}_{\tilde{B}_j'}(g)]$ is acquired using the computation denoted by (18) and (19).

$$\bar{\mu}_{\tilde{B}_j'}(g) = \min(UFS_j, \bar{\mu}_{\tilde{B}_j}(g)) \quad (18)$$

$$\underline{\mu}_{\tilde{B}_j'}(g) = \min(LFS_j, \underline{\mu}_{\tilde{B}_j}(g)) \quad (19)$$

However, in the event that multiple rules associated with either identical or different class labels in the consequent are fired, the final inference $\tilde{B}'$ is assessed by computing the union of IT2 inferences using (20).

$$\tilde{B}' = [\bigcup_{\forall j} \tilde{B}'_j] = [\bigcup_{\forall j} \overline{\tilde{B}}'_j, \bigcup_{\forall j} \underline{\tilde{B}}'_j] \quad (20)$$

where, $\bigcup$ denotes the union operator.

Finally, the type-reduction and defuzzification of $\tilde{B}'$ is executed using the Enhanced Karnik-Mendel (EKM) [59] algorithm to obtain C_{b^U} and C_{b^L}. Subsequently, the centroid C_e is determined by calculating the mean of C_{b^U} and C_{b^L}.

It is crucial to highlight that due to the presence of overlap among the data points of 2 or more classes, the acquired cluster centroids must lie in disjoint contiguous intervals for accurate classification of the input features $[f'_1, f'_2, ..., f'_N]$ into one of the S distinct classes (here, S = 4). Let, the interval for the j^{th} class centroid be $[C_{b_j^U}, C_{b_j^L}]$. Similarly, let the class centroids for neighboring classes j-1 and j+1 be denoted by $[C_{b_{j-1}^U}, C_{b_{j-1}^L}]$ and $[C_{b_{j+1}^U}, C_{b_{j+1}^L}]$ respectively. To ensure contiguous class boundaries, the following criteria are maintained for S-class classification.

i) $C_{b_{j-1}^L} < C_{b_{j-1}^U}$,

ii) $C_{b_{j-1}^U} = C_{b_j^L} < C_{b_j^U}$,

iii) $C_{b_j^U} = C_{b_{j+1}^L} < C_{b_{j+1}^U}$

The optimal class boundaries are acquired using random search algorithm [60] and their values are denoted in Section IV-D. Once, the contiguous class boundaries are maintained, the class inferred is j if the centroid value C_e acquired from EKM algorithm lies within the range $[C_{b_j^U}, C_{b_j^L}]$ (vide Appendix A.2).

D.4. Rank Assignment to Individuals with Respect to Different Levels of Creative Potential

Participants in the current cognitive task are categorized based on the number of experimental instances classified as High Creative (HCR). In other words, if a subject has r experimental instances identified as HCR, their ranking is determined using the following Creativity Potential Measure (CPM).

$$CPM = \frac{r}{R} \times 100\% \quad (21)$$

where, R denotes the total number of experimental instances for a specific participant. Once the CPM scores for all subjects are obtained, they are sorted in descending order. Then, each subject is assigned a rank based on its CPM score, with the highest score receiving the top rank.

IV. Experiments and Results of Brain Connectivity Based Cognitive Assessment of Creatvity

A. fNIRS Data Acquisition

The experiment was conducted at the Artificial Intelligence Laboratory of Jadavpur University in Kolkata, India. To capture the hemodynamic response of subjects during the current cognitive experiment, a whole-brain fNIRS device (NIRScout TM) manufactured by NIRx Medical Technologies, LLC, was employed. This device utilizes 8 infrared (IR) sources and 8 detectors, operating at a sampling rate of 7.81 Hz. The placement of the source-detector pairs, or optodes, on the subjects' scalps adhered to the 10-10

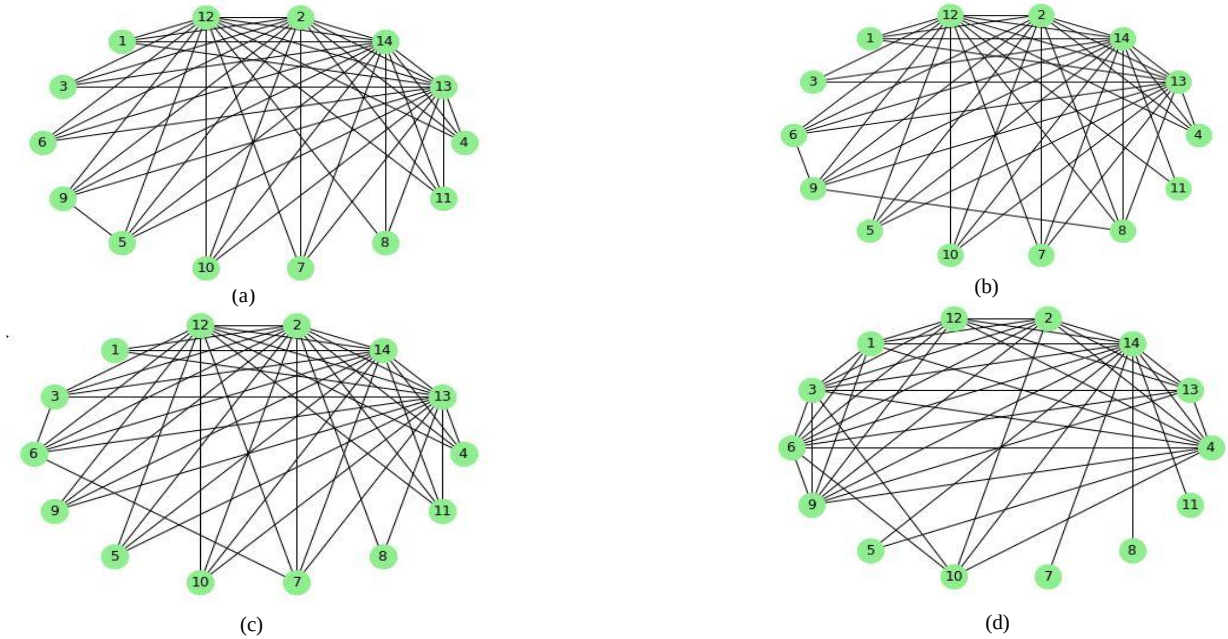

Fig. 11. Brain connectivity network of participants performing the MPF task: (a) Brain network of subject ID: 02 who could correctly solve the presented problem, (b) Brain network of subject ID: 23 who could moderately solve the presented problem, (c) Brain network of subject ID: 07 who could hardly solve the presented problem and (d) Brain network of subject ID: 20 who could not solve the presented problem

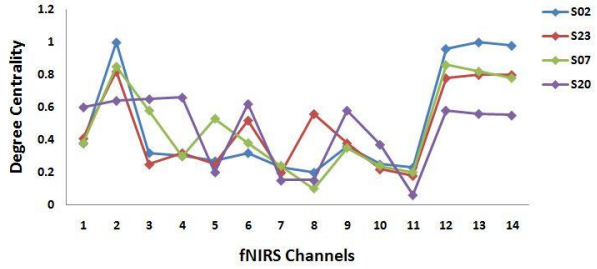

(a)

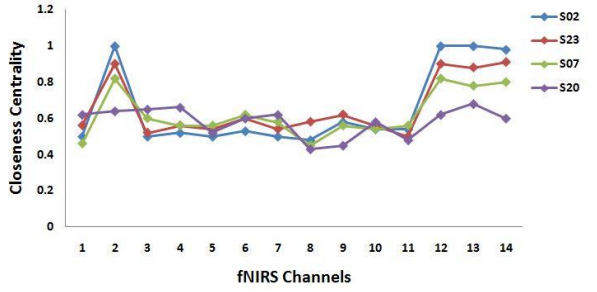

(b)

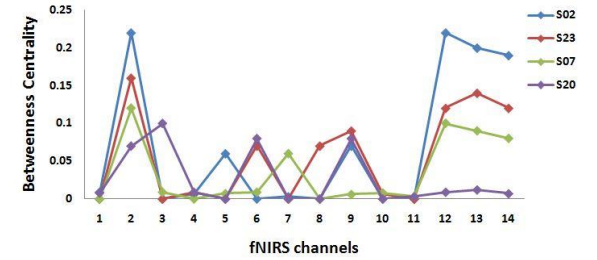

(c)

Fig. 12. Centrality based feature comparison for 4 degrees of creative ability (a) degree centrality analysis (b) closeness centrality analysis (c) betweenness centrality analysis

international placement system as shown in Fig. 9. The architecture of the montage for optode placement is portrayed in Fig. 10 and encompasses the pre-frontal, temporal, and parietal lobes. The rationale for opting for the afore-said montage architecture is derived from the acknowledgment that a spatial reasoning task engages the working memory and executive functions of the brain [61]-[62]. A total of 64 channels were generated by the optodes, and 14 channels were chosen based on the nearest-neighbor source-detector combination.

B. Participants

The said cognitive task involved the participation of 32 (engineering student) volunteers, consisting of 15 males and 17 females, all falling within the age range of 18 to 33 years. It is worth noting that all participants possessed normal or corrected-to-normal vision and had no previous history of neuropsychiatric or motor disorders. In accordance with the ethical guidelines and safety protocols related to the experiment, adherence to the Helsinki Declaration of 1970, revised in 2004, was maintained [63].

C. Cognitive Aspect of Brain Connectivity Features

The brain connectivity graphs for the current cognitive task have been obtained by the utilization of PC technique, to capture the interactions among different brain lobes. The connectivity patterns associated with each class label were extracted using the Networkx package [64] of Python 3 and are depicted in Fig. 11. To gauge the topological significance of specific lobes, a quantitative assessment has been conducted using centrality measures including degree, closeness, and betweenness. These measures facilitate the recognition of topologically central or hub lobes within the acquired brain graphs. The examination of brain topographic networks using individual centrality features is outlined below.

(a) DC Analysis: The Fig. 12 (a) illustrates the DC values of four subjects pertaining to HCR, MCR, LCR, and NCR classes for a single trial. Notably, for subject ID: 02 in the HCR class, the DC values are elevated over the right frontal (channel 2), right temporal (channel 12), and bilateral parietal (channels 13 and 14) regions. Additionally, a discernible trend is observed where the DC values decrease from HCR to LCR class for these specified regions. In contrast, for subjects in the NCR class, exemplified by subject ID: 20, there is no significant activation observed in the mentioned channels of the frontal, parietal, and temporal lobes. Nevertheless, moderately high DC values are evident in other nodes, such as channels 6 and 9 for MCR and channels 3 and 5 for LCR. This analysis suggests that relying solely on the DC measure provides only a partial understanding of the functional importance of nodes. Consequently, incorporating additional measures is essential to comprehensively quantify the distinct networks.

(b) CC Analysis: In Fig. 12 (b), the CC values for the same subjects utilized in the DC analysis are presented. Notably, for a subject in the HCR class, elevated CC values are evident over the right frontal (channel 2), right temporal (channel 12), and bilateral parietal (channels 13 and 14) regions. Furthermore, CC values for subjects in the MCR and LCR classes also show heightened values in these specified channels, with a discernible decrease in values from HCR to LCR classes. Conversely, subjects in the NCR class exhibit no significant activation in the aforementioned channels, as indicated by lower CC values. The CC analysis supports the conclusion that the regions with elevated values can be considered topologically central. This centrality implies that these regions can effectively interact with other nodes within the network through a small number of links [35].

(c) BC Analysis: The results of the BC analysis, as illustrated in Fig. 12 (c), underscore the same regions for each class as identified through CC-based evaluation. The manifestation of high BC values in these identified lobes suggests their effective functional integration among various brain regions [35]-[36].

Hence, the centrality-based feature analysis mentioned above supports the proposition that, for spatial reasoning, the actively engaged brain regions include the right anterior prefrontal cortex (BA 10 corresponding to channel 2), right posterior middle temporal gyrus (BA 21 corresponding to channel 12), and bilateral regions of the posterior

TABLE I
COMPARATIVE STUDY OF CLASSIFIER PERFORMANCE WITH RESPECT TO TRADITIONAL METHODS

Classifiers with optimal parameter settings	CA (%)	F1 (%)	Run time complexity (ms)
DCNN [65]	76.32	75.26	192.36
Chebnet [66]	78.02	78.32	156.20
GCN [37]	80.83	81.47	87.46
DGCN [67]	83.28	83.86	120.34
CayleyNet [68]	85.12	85.05	158.87
GAT [69]	88.70	89.27	96.12
AGCN [70]	91.95	92.50	95.46
Proposed GC-IT2FN	**97.54**	**97.72**	**99.06**

TABLE II
COMPARATIVE STUDY OF CLASSIFIER PERFORMANCE WITH RESPECT TO STATE-OF-THE-ART-METHODS

Classifiers with optimal parameter settings	CA (%)	F1 (%)	Run time complexity (ms)
GCNN-LSTM [71]	87.78	88.11	302.86
ASGCNN [72]	90.23	89.70	372.45
GAT + BiLSTM [73]	91.34	91.63	421.23
CapsualGNN [74]	92.97	92.74	134.70
CNN-AE + IT2FR-GWO [75]	94.56	94.83	125.60
AEGCN [76]	93.25	93.61	248.27
NCGNN [77]	95.12	95.36	143.18
Proposed GC-IT2FN	**97.54**	**97.72**	**99.06**

supramarginal gyrus (BA 40 corresponding to channels 13 and 14). These findings align with existing literature [23], [29], [61]-[62]. Additionally, a noticeable trend emerges, indicating a diminishing activation in the aforementioned Brodmann Areas (BAs) as the level of creative ability decreases from high to low levels.

D. Optimization of Classifier Parameters

Fine-tuning various parameters of the GC-IT2FN classifier model is essential for ensuring both its robustness and classification accuracy. This process is achieved by employing the random search algorithm, known for efficiently exploring the search space with minimal computational cost [60]. The model's performance has been evaluated by a 10-fold cross-validation across various sets of parameter configurations, where the dataset for each subject is partitioned into 10 disjoint sets or folds. For each combination of parameters, the model is trained on 9 folds and tested on the remaining 1 fold. This process is repeated in 10 iterations, rotating the test fold. Hence, both the training and testing sets for each subject comprise samples from the same individual, although they are distinct in each iteration. Upon attaining the highest accuracy level with all candidate settings, the best configuration is subsequently applied to the test set. The optimal parameter values of GC-IT2FN classifier utilized for the current

TABLE III
ABLATION STUDY OF THE PROPOSED CLASSIFIER

Variation in Classifier Modules	CA (%)	F1 (%)
GCN	89.47	90.03
IT2FS	88.78	88.55
Attention + GCN	92.50	92.83
GCN + IT2FS	94.36	94.64
Proposed GC-IT2FN	**97.54**	**97.72**

TABLE IV
COMPARATIVE STUDY OF DIFFERENT FORMULATIONS OF BRAIN CONNECTIVITY NETWORKS WITH RESPECT TO CA (%)

Formulations of brain connectivity network	Class Labels			
	HCR	MCR	LCR	NCR
MSC	89.52	90.04	89.73	90.11
PLV	91.36	92.46	91.60	92.29
PLI	92.08	91.22	91.54	92.16
KNN	94.20	93.75	93.85	94.32
MI	95.67	95.43	95.91	95.76
PC	**97.87**	**97.32**	**96.92**	**98.03**

experiment include: $E'=2$, $T=128$, $N=64$, $\eta=1.8$, $C_{b_{NCR}^{L}}=9.27$, $C_{b_{NCR}^{U}}=C_{b_{LCR}^{L}}=23.70$, $C_{b_{LCR}^{U}}=C_{b_{MCR}^{L}}=43.02$, $C_{b_{MCR}^{U}}=C_{b_{HCR}^{L}}=72.56$, and $C_{b_{HCR}^{U}}=97.25$.

V. PERFORMANCE ANALYSIS OF THE PROPOSED CLASSIFIER MODEL

A. Relative Performance Analysis of the Proposed GC-IT2FN Classifier with Respect to Traditional Algorithms

The performance of the GC-IT2FN classifier is analyzed with the traditional algorithms using i) classification accuracy (CA) and ii) F1-score whose mathematical equations are illustrated by (22-23).

$$CA=\frac{T_P+T_N}{T_P+T_N+F_P+F_N} \tag{22}$$

$$F1=\frac{2\times precison\times recall}{precision+recall} \tag{23}$$

where, T_P, T_N, F_P, F_N represents the number of true positives, true negatives, false positives and false negatives respectively, $precison=\frac{T_P}{T_P+F_P}$ and $recall=\frac{T_P}{T_P+F_N}$.

Table I clearly demonstrates the remarkable precision with which the proposed algorithm classifies the desired class labels. Notably, the results achieved by GC-IT2FN far surpass those of the traditional techniques. Moreover, Table I highlights the run-time complexity of the proposed classifier, which stands at an impressively low 99.06 ms, making it notably faster than the majority of competitive techniques.

TABLE V
EFFECT OF DIFFERENT ACTIVATION FUNCTIONS ON THE PROPOSED MODEL WITH RESPECT TO CA (%)

Activation Functions	Class Labels			
	HCR	MCR	LCR	NCR
Sigmoid [83]	79.60	79.48	80.03	79.76
Tanh [84]	81.05	80.87	80.96	81.12
ReLU [85]	82.90	83.36	82.82	83.20
Leaky ReLU [86]	84.55	85.14	85.06	84.61
ELU [87]	86.34	86.17	85.78	85.97
SELU [88]	87.16	87.38	87.42	87.52
Swish [89]	89.11	88.97	89.20	88.83
ELiSH [90]	92.07	91.88	92.15	91.72
Mish [91]	93.63	93.47	94.03	93.68
Logish	**97.87**	**97.32**	**96.92**	**98.03**

TABLE VI
EFFECT OF REDUCING THE AREA UNDER THE FOU ON CLASSIFIER PERFORMANCE

Class Labels	Varying Classifier Architecture			
	GCN + IT2FS with original FOU		GCN + IT2FS with modified FOU	
	CA (%)	F1 (%)	CA (%)	F1 (%)
HCR	92.83	93.25	**97.87**	**98.12**
MCR	93.14	92.90	**97.32**	**97.08**
LCR	92.56	92.77	**96.92**	**97.25**
NCR	93.12	93.23	**98.03**	**98.43**

B. Relative Performance Analysis of the Proposed GC-IT2FN Classifier with respect to State-of-the-Art (SOTA) Algorithms

The performance evaluation of the GC-IT2FN classifier has been conducted by comparing it with recent SOTA techniques, which include various hybrid models utilized for classifying brain connectivity features. The outcomes of this comparative analysis are presented in Table II. The results clearly demonstrate that the proposed classifier surpasses the performance of the SOTA techniques by a substantial margin. Additionally, the run time complexity of the proposed technique is notably lower in comparison to all the hybrid methods.

C. Ablation Study of the Proposed GC-IT2FN Classifier

A comprehensive ablation study has been conducted on the proposed GC-IT2FN classifier to assess the influence of its individual modules on overall performance. In this analytical process, the architecture of the proposed model underwent systematic modifications through the removal of specific modules, and the corresponding results are detailed in Table III. It is apparent from this table that both the CA and F1-score values decline when either the GCN or IT2FS classifier is utilized in isolation for the classification task. Conversely, the inclusion of the attention mechanism to the GCN model leads to a significant improvement in both CA and F1-score. Furthermore, employing both GCN and IT2FS results in noticeable enhancement in CA and F1-score. Notably, the highest CA and F1-score values are achieved when all three modules of GC-IT2FN (i.e., attention, GCN, and IT2FN) are utilized together. Thus, the findings from this table underscore that excluding any single unit results in a noteworthy decrease in the overall performance of the proposed model.

D. Effect of Different Formulations of Brain Connectivity Network on Classifier Performance

The performance of the proposed classifier is assessed in comparison to brain connectivity network construction based on the PC method. This evaluation includes several standard methods for constructing brain connectivity networks, such as Magnitude Squared Coherence (MSC) [78], Phase Locking Value (PLV) [79], Phase Lag Index (PLI) [80], K-Nearest Neighbor (KNN) [81], and Mutual Information (MI) [82]. The outcomes of this comparative analysis are detailed in Table IV, revealing a noteworthy improvement in the proposed classifier's performance when employing PC-based brain connectivity network construction in contrast to the competitor techniques.

E. Influence of Different Activation Functions on Classifier Performance

Table V presents the outcomes of CA and F1-score variations in GC-IT2FN concerning different activation functions. The table clearly indicates that the proposed classifier achieves optimal results when the Logish activation function is employed.

F. Effect of Reducing the Area under the FOU on Classifier Performance

The effect of reducing the FOU using the modified LMF (as discussed in Section III-D) is compared against the traditional FOU formulation produced by considering the union of 10 Type-1 MFs obtained from 10 experimental days. The results of this comparison are tabulated in Table VI. It is evident from the table that the proposed approach of FOU reduction significantly improves both the CA and F1-score compared to the classical approach.

G. Influence of Different Brain Connectivity Features on Classifier Perfromance

The performance of the proposed classifier is evaluated with respect to the variation in three centrality based features: DC, CC and BC. It is observed from Table VII that though CC+BC, DC+BC and BC are able to provide a fairly high F1-score value, DC+CC+BC yields the highest F1-score in comparison to the other feature combinations.

H. Ranking of Subjects on the Basis of Scientific Creative Potential

Each subject's rank is determined by initially calculating their CPM score, denoted in (21), and arranging them in descending order. Following this arrangement, ranks are assigned to each subject based on their CPM score, with the highest CPM score receiving the top rank. In Table VIII, the ranks of the 10 subjects are presented instead of the entire cohort due to space constraints.

TABLE VII
COMPARATIVE STUDY OF DIFFERENT CONNECTIVITY FEATURES WITH RESPECT TO F1-SCORE (%)

Centrality Features	Class Labels			
	HCR	**MCR**	**LCR**	**NCR**
DC	93.62	92.87	93.30	93.08
CC	94.03	93.40	94.21	94.15
BC	95.27	95.74	95.45	95.92
DC+CC	94.88	94.51	94.72	94.60
DC+BC	96.20	96.02	96.11	96.33
CC+BC	96.75	96.81	96.25	97.42
DC+BC+CC	**98.12**	**97.08**	**97.25**	**98.43**

I. Statistical Validation of the Proposed GC-IT2FN Using Friedman's Test

To statistically validate the proposed algorithm, the Friedman's 2-way non-parametric statistical test [92] has been utilized for the present application. This test assigns the lowest rank to the best-performing algorithm. The Friedman statistic, denoted by χ_F^2 is computed for *(k-1)* degrees of freedom using the following equation.

$$\chi_F^2 = \frac{12N}{k(k+1)}\left[\sum_{a=1}^{k} R_a^2 - \frac{k(k+1)^2}{4}\right] \quad (24)$$

where, N represents the number of datasets (i.e., the number of creative classes), k indicates the number of classifier algorithms and R_a portrays the mean rank of the p^{th} algorithm pertaining to the q^{th} dataset. The results of the Friedman's test with respect to all classification metrics for $N = 4$ and $k = 8$ has been portrayed in Table IX. It is apparent from this table that the Friedman statistic $\chi_F^2 = 27.20 > \chi_{7,0.95}^2 = 14.07$, which depicts the chi-square value at 95% confidence level with 7 degrees of freedom. The outcomes of the Friedman test reveal the rejection of the null hypothesis, which asserts that all the algorithms exhibit equivalent performance. Consequently, the comparison of the algorithms must be performed by taking into account their respective ranks.

VI. CONCLUSION

Unraveling the creative capacities of individuals in the scientific domain poses a significant challenge within the realm of cognitive neuroscience. The present study makes a noteworthy contribution to this domain by utilizing fNIRS data, with a focus on evaluating the levels of creative aptitude through brain connectivity analysis. Such an analysis, centered on centrality features (i.e., degree, closeness, and betweenness), reveals the active engagement of the right anterior prefrontal cortex (BA 10), right posterior middle temporal gyrus (BA 21), and bilateral regions of the posterior supramarginal gyrus (BA 40) during the performance of a paper folding task. Subsequently, the centrality based features are classified using a novel GC-IT2FN classifier, demonstrating precise identification of desired class labels related to creative ability and superior performance compared to its competitors.

TABLE VIII
RANK OF 10 SUBJECTS BASED ON CLASSIFICATION RESULTS

Subject ID	CPM (%)	Rank
S27	**83.50**	**1**
S02	78.45	2
S11	76.52	3
S05	69.27	4
S08	69.11	5
S30	65.50	6
S23	59.47	7
S18	59.38	8
S09	55.29	9
S03	51.05	10

TABLE IX
STATISTICAL VALIDATION OF THE PROPOSED GC-IT2FN USING FRIEDMAN'S TEST

Classifiers Algorithms	R_a	χ_F^2
DCNN	8	**27.20 (Null Hypothesis is Rejected)**
Chebnet	6.75	
GCN	6	
DGCN	3.87	
CayleyNet	5.25	
GAT	3	
AGCN	2.12	
Proposed GC-IT2FN	**1**	

A captivating application of the proposed scheme involves identifying creative individuals for potential placement in various research-oriented departments in industrial sectors based on their different ranks of creative ability. For example, an individual exhibiting high creativity could be appointed to roles such as Advanced Data Analyst or Innovation Manager, where the demand for groundbreaking ideas and inventive problem-solving is paramount. A person with medium creative abilities might find a fitting role as a Research Assistant, contributing to the execution of research projects with a balance of structured methodologies and adaptable problem-solving. Meanwhile, someone with lower creative inclinations could be well-suited for a position like Quality Control Analyst, where attention to established protocols and meticulous adherence to quality standards is essential. Furthermore, the current study also nurtures the possibility of drawing biological inspiration for the creation of computational models of scientific creativity. The future scope of the proposed work may involve assessing the creative potential of individuals by exploring other cognitive phenomena that influence creative ideation in the scientific domain, such as inductive learning, analogical reasoning, and the like.

References

[1] M.A. Boden, *The creative mind: Myths and mechanisms*, Routledge, 2004.

[2] J.C. Kaufman and R.J. Sternberg, eds., *The Cambridge handbook of creativity*, Cambridge University Press, 2019.

[3] S. Acar, and M.A. Runco, "Divergent thinking: New methods, recent research, and extended theory", *Psychology of Aesthetics, Creativity, and the Arts*, vol. 13, no. 2, p.153, 2019.

[4] L. Ghosh, R. Kar, A. Konar, A. Chakraborty, and A. K. Nagar, "Identification of Brain Activation Regions in Inductive Learning Based Scientific Creativity Test," *In 2018 IEEE Symposium Series on Computational Intelligence (SSCI)*, pp. 950-957, 2018.

[5] S. Ghosh, L. Ghosh, A. Konar and A.K. Nagar, "Assessment of Subjective Creativity Skill Using EEG Induced Capsule Network", In *2020 IEEE Symposium Series on Computational Intelligence (SSCI)*, pp. 3107-3114, 2020.

[6] P.Esling and N. Devis, "Creativity in the era of artificial intelligence", *arXiv preprint arXiv:2008.05959*, 2020.

[7] M. Palmiero, and N. Srinivasan, "Creativity and spatial ability: a critical evaluation," *Cognition, experience and creativity*, pp.189-214, 2015.

[8] H. Burte, A.L. Gardony, A. Hutton, and H.A. Taylor, "Make-A-Dice Test: Assessing the intersection of mathematical and spatial thinking", *Behavior research methods*, vol. 51, pp.602-638, 2019.

[9] K.S. Mix, and M.T. Battista, eds., *Visualizing mathematics: The role of spatial reasoning in mathematical thought*, Springer, 2018.

[10] D. Novitasari, D.K.Risfianty, T.W. Triutami, N.P. Wulandari and R.Y. Tyaningsih, "The relation between spatial reasoning and creativity in solving geometric problems", *In Journal of Physics: Conference Series*, Vol. 1776, No. 1, p. 012007, *IOP Publishing*, 2021.

[11] J. Suh, and J.Y. Cho, "Linking spatial ability, spatial strategies, and spatial creativity: A step to clarify the fuzzy relationship between spatial ability and creativity," *Thinking Skills and Creativity*, vol. 35, p.100628, 2020.

[12] H.J. Kell, D. Lubinski, C.P. Benbow, and J.H. Steiger, "Creativity and technical innovation: Spatial ability's unique role," *Psychological science*, vol. 24, no. 9, pp.1831-1836, 2013.

[13] A.C. Rule, "Spatial thinking skills and STEM connections: How does this issue address them?", *Journal of STEM Arts, Crafts, and Constructions*, vol. 1, no. 2, p.1, 2016.

[14] M. Hegarty, R.D. Crookes, D. Dara-Abrams, and T.F.Shipley, "Do all science disciplines rely on spatial abilities? Preliminary evidence from self-report questionnaires", *In Spatial Cognition VII: International Conference, Spatial Cognition 2010*, Mt. Hood/Portland, OR, USA, Proceedings 7 , pp. 85-94, Springer Berlin Heidelberg, August 15-19, 2010.

[15] Z. Hawes. and D. Ansari, "What explains the relationship between spatial and mathematical skills? A review of evidence from brain and behavior", *Psychonomic bulletin & review*, vol. 27, pp.465-482, 2020.

[16] L. Glass, F. Krueger, J. Solomon, V. Raymont, and J. Grafman, "Mental paper folding performance following penetrating traumatic brain injury in combat veterans: a lesion mapping study", *Cerebral Cortex*, vol. 23, no. 7, pp.1663-1672, 2013.

[17] L. Wang, C. Cao, X. Zhou, and C. Qi, "Spatial abilities associated with open math problem solving," *Applied Cognitive Psychology*, vol. 36, no. 2, pp.306-317, 2022.

[18] M. Yu, J. Cui, L. Wang, X. Gao, Z. Cui, and X. Zhou, "Spatial processing rather than logical reasoning was found to be critical for mathematical problem-solving," *Learning and Individual Differences*, vol. 100, p.102230, 2022.

[19] S. Manimozhi, and N. Vasuki, "Effect of Interventional Strategies to Learn Geometry-A comparative study," *JETT*, vol. 4, pp.181-186, 2022.

[20] J. Adams, I. Resnick, and T. Lowrie, "Supporting senior high-school students' measurement and geometry performance: Does spatial training transfer to mathematics achievement?," *Mathematics Education Research Journal*, vol 35, no. 4, pp.879-900, 2023.

[21] S.F Dahm, and C. Draxler, "Mental Paper Folding Revisited: The Involvement of Visual Action Imagery," *Psych*, vol. 5, no. 1, pp.14-25, 2022.

[22] C. Goumopoulos, and N. Potha, "Mental fatigue detection using a wearable commodity device and machine learning," *Journal of Ambient Intelligence and Humanized Computing*, vol. 14, no. 8, pp.10103-10121, 2023.

[23] Y. Gazes, S. Lee, J. Sakhardande, A. Mensing, Q. Razlighi, A. Ohkawa, M. Pleshkevich, L. Luo, and C. Habeck, "fMRI-guided white matter connectivity in fluid and crystallized cognitive abilities in healthy adults", *Neuroimage*, vol. 215, p.116809, 2020.

[24] S. Xu, Y. Li, and J. Liu, "The neural correlates of computational thinking: Collaboration of distinct cognitive components revealed by fMRI", *Cerebral Cortex*, vol. 31, no. 12, pp.5579-5597, 2021.

[25] C.Y. Tang, E.L. Eaves, J.C. Ng, D.M. Carpenter, X. Mai, D.H. Schroeder, C.A. Condon, R. Colom, and R.J. Haier, "Brain networks for working memory and factors of intelligence assessed in males and females with fMRI and DTI", *Intelligence*, vol. 38, no.3, pp.293-303, 2010.

[26] C. Habeck, J. Steffener, D. Barulli, Y. Gazes, Q. Razlighi, D. Shaked, T. Salthouse, and Y. Stern, "Making cognitive latent variables manifest: distinct neural networks for fluid reasoning and processing speed," *Journal of cognitive neuroscience*, vol. 27, no. 6, pp.1249-1258, 2015.

[27] B. Milivojevic, B.W. Johnson, J.P. Hamm, and M.C. Corballis, "Non-identical neural mechanisms for two types of mental transformation: event-related potentials during mental rotation and mental paper folding," *Neuropsychologia*, vol. 41, no. 10, pp.1345-1356, 2003.

[28] C. Hilton, L. Raddatz, and K. Gramann, "A general spatial transformation process? Assessing the neurophysiological evidence on the similarity of mental rotation and folding," *Neuroimage: Reports*, vol. 2, no. 2, p.100092, 2022.

[29] S. Ghosh, A. Konar, and A.K. Nagar, "Decoding Subjective Creativity Skill from Visuo-Spatial Reasoning Ability Using Capsule Graph Neural Network," In *2021 International Joint Conference on Neural Networks (IJCNN)*, pp. 1-8, 2021.

[30] C. Brunner, M. Billinger, M. Seeber, T.R. Mullen, and S. Makeig, "Volume conduction influences scalp-based connectivity estimates," *Front Comput Neurosci*, vol. 10, no. 121, 2016.

[31] F. Wang, X. Zhang, R. Fu and G. Sun, "EEG characteristic analysis of coach bus drivers based on brain connectivity as revealed via a graph theoretical network," *RSC advances*, vol. 8, no. 52, pp.29745-29755, 2018.

[32] A. Dudáš, "Graphical representation of data prediction potential: correlation graphs and correlation chains," *The Visual Computer*, pp.1-14, 2024.

[33] N. Masuda, M. Sakaki, T. Ezaki, and T. Watanabe, "Clustering coefficients for correlation networks," *Frontiers in neuroinformatics*, vol. 12, p.7, 2018.

[34] Z. Šverko, M. Vrankić, S. Vlahinić, and P. Rogelj, "Complex Pearson correlation coefficient for EEG connectivity analysis," *Sensors*, vol. 22, no. 4, p.1477, 2022.

[35] M. Rubinov, and O. Sporns, "Complex network measures of brain connectivity: uses and interpretations," *Neuroimage*, vol. 52, no. 3, pp.1059-1069, 2010.

[36] A. Fornito, A. Zalesky, E. and Bullmore, *Fundamentals of brain network analysis*, Academic press, 2016.

[37] T.N. Kipf, and M. Welling, "Semi-supervised classification with graph convolutional networks," *arXiv preprint arXiv:1609.02907*, 2016.

[38] Z. Zhang, P. Cui, and W. Zhu, "Deep learning on graphs: A survey," *IEEE Transactions on Knowledge and Data Engineering*, vol. 34, no. 1, pp.249-270, 2020.

[39] S. Zhang, H. Tong, J. Xu, and R. Maciejewski, "Graph convolutional networks: a comprehensive review," *Computational Social Networks*, vol. 6, no. 1, pp.1-23, 2019.

[40] M. Chen, Z. Wei, Z. Huang, B. Ding, and Y. Li, "Simple and deep graph convolutional networks," In *International conference on machine learning*, pp. 1725-1735, PMLR, 2020.

[41] R. Huang, K.S. Hong, D. Yang, and G. Huang, "Motion artifacts removal and evaluation techniques for functional near-infrared spectroscopy signals: a review," *Frontiers in Neuroscience*, vol. 16, p.878750, 2022.

[42] P. Raggam, G. Bauernfeind, and S.C. Wriessnegger, "NICA: a novel toolbox for near-infrared spectroscopy calculations and analyses," *Frontiers in Neuroinformatics*, vol. 14, p.26, 2020.

[43] M. Laha, A. Konar, P. Rakshit, and A.K. Nagar, "Exploration of subjective color perceptual-ability by EEG-induced type-2 fuzzy classifiers," *IEEE Transactions on Cognitive and Developmental Systems*, vol. 12, no. 3, pp.618-635, 2019.

[44] M. Laha, A. Konar, P. Rakshit, and A.K. Nagar, "Hemodynamic analysis for olfactory perceptual degradation assessment using generalized type-2 fuzzy regression," *IEEE Transactions on Cognitive and Developmental Systems*, vol. 14, no. 3, pp.618-635, 2021.

[45] H. Zhu, H. Zeng, J. Liu, and X. Zhang, "Logish: A new nonlinear nonmonotonic activation function for convolutional neural network," *Neurocomputing*, vol. 458, pp. 490–499, 2021.

[46] D. Wu, and J.M. Mendel, "A vector similarity measure for linguistic approximation: Interval type-2 and type-1 fuzzy sets," *Information Sciences*, vol. 178, no. 2, pp.381-402, 2008.

[47] D. Wu, "On the fundamental differences between interval type-2 and type-1 fuzzy logic controllers," *IEEE Transactions on Fuzzy Systems*, vol. 20, no. 5, pp.832-848, 2012.

[48] H. Burte, A.L. Gardony, A. Hutton, and H.A. Taylor, "Knowing when to fold'em: Problem attributes and strategy differences in the Paper Folding test," *Personality and Individual Differences*, vol. 146, pp.171-181, 2019.

[49] J. Ainooson, and M. Kunda, "A Computational Model for Reasoning About the Paper Folding Task Using Visual Mental Images," In *CogSci*, 2017.

[50] R.J.Cooper, J. Selb, L. Gagnon, D. Phillip, H.W. Schytz, H.K. Iversen, M. Ashina, and D.A. Boas, "A systematic comparison of motion artifact correction techniques for functional near-infrared spectroscopy," *Frontiers in neuroscience*, vol. 6, p.147, 2012.

[51] H.D. Nguyen, S.H. Yoo, M.R. Bhutta, and K.S. Hong, "Adaptive filtering of physiological noises in fNIRS data," *Biomedical engineering online*, vol. 17, pp.1-23, 2018.

[52] S. Kohno, I. Miyai, A. Seiyama, I. Oda, A. Ishikawa, S. Tsuneishi, T. Amita, and K. Shimizu, "Removal of the skin blood flow artifact in functional near-infrared spectroscopic imaging data through independent component analysis," *Journal of biomedical optics*, vol. 12, no. 6, pp.062111-062111, 2007.

[53] M.A. Rahman, M.S. Uddin, and M. Ahmad, "Modeling and classification of voluntary and imagery movements for brain–computer interface from fNIR and EEG signals through convolutional neural network," *Health Information Science and Systems*, vol. 7, no. 1, p.22, 2019.

[54] A. Kachenoura, L. Albera, L. Senhadji, and P. Comon, "ICA: a potential tool for BCI systems," *IEEE Signal Processing Mag*., vol. 25, no. 1, pp. 57-68, 2008.

[55] Z. Zhao, A. Kleinhans, G. Sandhu, I. Patel, and K.P. Unnikrishnan, "Capsule networks with max-min normalization," *arXiv preprint arXiv:1903.09662*, 2019.

[56] B.C. Van Wijk, C.J. Stam, and A. Daffertshofer, "Comparing brain networks of different size and connectivity density using graph theory," *PloS one*, vol. 5, no. 10, p.e13701, 2010.

[57] K. Qin, D. Lei, W.H. Pinaya, N. Pan, W. Li, Z. Zhu, J.A. Sweeney, A. Mechelli, and Q. Gong, "Using graph convolutional network to characterize individuals with major depressive disorder across multiple imaging sites," *EBioMedicine*, vol 78, 2021.

[58] A. Saha, A. Konar, and A.K. Nagar, "EEG analysis for cognitive failure detection in driving using type-2 fuzzy classifiers," *IEEE Transactions on Emerging Topics in Computational Intelligence*, vol. 1, no. 6, pp.437-453, 2017.

[59] D. Wu, and J.M. Mendel, "Enhanced karnik--mendel algorithms," *IEEE transactions on fuzzy systems*, vol. 17, no. 4, pp.923-934, 2008.

[60] J. Bergstra and Y. Bengio, "Random search for hyper-parameter optimization", *The Journal of Machine Learning Research*, vol. 13, no. 1, pp. 281–305, 2012.

[61] Z. Hawes, J. Moss, B. Caswell, J. Seo, and D. Ansari, "Relations between numerical, spatial, and executive function skills and mathematics achievement: A latent-variable approach", *Cognitive Psychology*, vol. 109, pp.68-90, 2019.

[62] A. Miyake, N.P. Friedman, D.A. Rettinger, P. Shah, and M. Hegarty, "How are visuospatial working memory, executive functioning, and spatial abilities related? A latent-variable analysis", *Journal of experimental psychology: General*, vol. 130, no. 4, p.621, 2001.

[63] General Assembly of the World Medical Association, "World Medical Association Declaration of Helsinki: ethical principles for medical research involving human subjects," *The Journal of the American College of Dentists*, vol. 81, no. 3, pp.14-18, 2014.

[64] A. A. Hagberg, D. A. Schult, and P. J. Swart, "Exploring network structure, dynamics, and function using networkx," *In Proceedings of the 7th Python in Science Conference (SciPy2008)*, 2008.

[65] J. Atwood, and D. Towsley, "Diffusion-convolutional neural networks," *Advances in neural information processing systems*, vol. 29, 2016.

[66] M. Defferrard, X. Bresson, and P. Vandergheynst,"Convolutional neural networks on graphs with fast localized spectral filtering," *In Proceedings of the 30th International Conference on Neural Information Processing Systems* , pp. 3844-3852, 2016.

[67] C. Zhuang and Q. Ma, "Dual graph convolutional networks for graph-based semi-supervised classification," In *Proceedings of the 2018 World Wide Web Conference*, pp. 499-508, 2018.

[68] R. Levie, F. Monti, X. Bresson, and M.M. Bronstein, "Cayleynets: Graph convolutional neural networks with complex rational spectral filters," *IEEE Transactions on Signal Processing*, vol. 67, no. 1, pp.97-109, 2018.

[69] P. Veličković, G. Cucurull, A. Casanova, A. Romero, P. Lio and Y. Bengio, " Graph attention networks," *arXiv preprint arXiv:1710.10903*, 2017.

[70] F. Ma, F. Gao, J. Sun, H. Zhou, and A. Hussain, "Attention graph convolution network for image segmentation in big SAR imagery data," *Remote Sensing*, vol. 11, no. 21, p.2586, 2019.

[71] K. Masood, and R. Kashef, "Integrating graph convolutional networks (gcnns) and long short-term memory (lstm) for efficient diagnosis of autism," In *International Conference on Artificial Intelligence in Medicine*, pp. 110-121, Cham: Springer International Publishing, 2022.

[72] H. Chang, B. Liu, Y. Zong, C. Lu, and X. Wang, "EEG-Based Parkinson's Disease Recognition Via Attention-based Sparse Graph Convolutional Neural Network," *IEEE Journal of Biomedical and Health Informatics*, 2023.

[73] J. He, J. Cui, G. Zhang, M. Xue, D. Chu, and Y. Zhao, "Spatial–temporal seizure detection with graph attention network and bi-directional LSTM architecture," *Biomedical Signal Processing and Control*, vol. 78, p.103908, 2022.

[74] Y. Wang, H. Wang, H. Jin, X. Huang, and X. Wang, "Exploring graph capsual network for graph classification," *Information Sciences*, vol. 581, pp.932-950, 2021.

[75] A. Shoeibi, N. Ghassemi, M. Khodatars, P. Moridian, A. Khosravi, A. Zare, J.M. Gorriz, A.H. Chale-Chale, A. Khadem, and U. Rajendra Acharya, "Automatic diagnosis of schizophrenia and attention deficit hyperactivity disorder in rs-fMRI modality using convolutional autoencoder model and interval type-2 fuzzy regression", *Cognitive Neurodynamics*, vol. 17, no. 6, pp.1501-1523, 2023.

[76] M. Ma, S. Na, and H. Wang, "AEGCN: An autoencoder-constrained graph convolutional network," *Neurocomputing*, vol. 432, pp.21-31, 2021.

[77] R. Yang, W. Dai, C. Li, J. Zou, and H. Xiong, "Ncgnn: Node-level capsule graph neural network for semisupervised classification," *IEEE Transactions on Neural Networks and Learning Systems*, 2022.

[78] X. Shan, J. Cao, S. Huo, L. Chen, P.G. Sarrigiannis, and Y. Zhao, "Spatial–temporal graph convolutional network for Alzheimer classification based on brain functional connectivity imaging of electroencephalogram," *Human Brain Mapping*, vol. 43, no. 17, pp.5194-5209, 2022.

[79] H. Wu, and J. Liu, "A Multi-stream Deep Learning Model for EEG-based Depression Identification," In *2022 IEEE International Conference on Bioinformatics and Biomedicine (BIBM)*, pp. 2029-2034, 2022.

[80] J. Wang, Y. Song, Q. Gao, and Z. Mao, "Functional brain network based multi-domain feature fusion of hearing-Impaired EEG emotion identification," *Biomedical Signal Processing and Control*, vol. 85, p.105013, 2023.

[81] S. Bloemheuvel, J. van den Hoogen, and M. Atzmueller, "Graph construction on complex spatiotemporal data for enhancing graph neural network-based approaches," *International Journal of Data Science and Analytics*, pp.1-18, 2023.

[82] M. Wu, R. Ouyang, C. Zhou, Z. Sun, F. Li, and P. Li, "A study on the combination of functional connection features and Riemannian manifold in EEG emotion recognition," *Frontiers in Neuroscience*, vol. 17, 2023.

[83] J. Turian, J. Bergstra, and Y. Bengio, "Quadratic features and deep architectures for chunking," *in Proceedings of Human Language Technologies: The 2009 Annual Conference of the North American Chapter of the Association for Computational Linguistics*, vol. Companion Volume:, pp. 245–248, 2009.

[84] B. Karlik and A. Vehbi, "Performance Analysis of Various Activation Functions in Generalized MLP Architectures of Neural Networks," *International Journal of Artificial Intelligence and Expert Systems (IJAE)*, vol. 1, no. 4, pp. 111–122, 2011.

[85] V. Nair and G. E. Hinton, "Rectified linear units improve restricted boltzmann machines," *Haifa*, pp. 807–814, 2010.

[86] A.K Dubey, and V. Jain, "Comparative study of convolution neural network's relu and leaky-relu activation functions," In *Applications of Computing, Automation and Wireless Systems in Electrical Engineering: Proceedings of MARC 2018*, pp. 873-880, Springer Singapore, 2019.

[87] D.A. Clevert, T. Unterthiner, and S. Hochreiter, "Fast and accurate deep network learning by exponential linear units (elus)," *arXiv preprint arXiv:1511.07289*, 2015.

[88] G. Klambauer, T. Unterthiner, A. Mayr, and S. Hochreiter, "Self-Normalizing Neural Networks," *arXiv*, 2017.

[89] P. Ramachandran, B. Zoph, and Q. V. Le, "Searching for Activation Functions," *ArXiv*, 2017.

[90] M. Basirat, P. M. Roth, "The Quest for the Golden Activation Function," *arXiv* , 2018.

[91] D. Misra, "Mish: A Self Regularized Non-Monotonic Neural Activation Function", *arXiv:1908.08681 [cs stat]*, Oct. 2019.

[92] J. Demsar, "Statistical Comparisons of Classifiers over Multiple Data Sets", *J. Machine Learning Research*, vol. 7, pp. 1-30, 2006.

[93] Appendix–https://drive.google.com/file/d/1Pi3FISsZmQjPMU4fRD4zZf3V1i2NRheG/view?usp=sharing

Sayantani Ghosh received her B.Tech. degree in Electronics and Communication Engineering from Dr. Sudhir Chandra Sur Degree Engineering College, Kolkata, India in 2015, and her M. Tech. degree in Intelligent Automation and Robotics (IAR) from the department of Electronics and Tele-Communication Engineering, Jadavpur University, Kolkata in 2018. She is currently working towards the Ph.D. degree in Artificial Intelligence and Cognitive Neuroscience from Jadavpur University under the guidance of Prof. Amit Konar. She is the recepient of 'Jodh Ishwar Singh (JIS) Sanman for Academic Excellence' by JIS Group, West Bengal, India in 2015, IEEE Brain Best Paper Award Runner Up by IEEE Symposium Series on Computational Intelligence (SSCI), Florida, USA in 2021 and IEEE Best Paper Award in the track Signal Processing and Computing Systems by International Conference on Computers and Devices for Communication (CODEC), Kolkata, India, in 2023. Her current research interests include Computational Creativity, Deep Learning, Brain-Computer Interfaces, Biological Underpinning of Perception and Scientific Creativity.

Amit Konar (SM' 2010) is currently a Professor in the department of Electronics and Tele-Communication Engineering, Jadavpur University, Kolkata, India. He earned his B.E. degree in Electronics and Tele-Communication Engineering from Indian Institute of Engineering Science and Technology (previously, Bengal Engineering College), Kolkata in 1983, his M.E. degree in Control Engineering, M. Phil. degree in System Modelling and Ph.D. degree in Artificial Intelligence, all from Jadavpur University in 1985, 1988 and 1994 respectively.

Dr. Konar is the author of 15 books including two popular texts, *Artificial Intelligence and Soft Computing: Behavioral and Cognitive Modeling of the Human Brain*, (CRC Press) in 2000 and *Computational Intelligence: Principles, Techniques and Applications*, (Springer) in 2005. He has published 35 peer-reviewed book chapters and over 100 research papers in leading international journals (including 29 IEEE Transactions), and over 250 research papers published in IEEE Flagship Conference proceeedings. He has supervised 29 Ph.D. theses and over 400 Masters theses, all in the broad area of Cognitive Neuro-science, AI and Robotics. Dr. Konar delivered keynote/tutorial speech in top flagship IEEE Conferences including WCCI-2020 and ICASSP-2016. He has been serving as the Associate Editor of IEEE TFS and IEEE TETCI for several years. Dr. Konar is currently the EIC of the Springer book series on Cognitive Intelligence and Robotics. He served as the Coordinator/Principal Investigator of several National level projects funded by Government of india and industries. His current research interest includes Cognitive Neuroscience, Type-2 Fuzzy Logic, Multi-agent Systems and Scientific Creativity.

Atulya K. Nagar is a Professor of Mathematical Sciences and is the Pro Vice-Chancellor (Research) at Liverpool Hope University, United Kingdom. He is responsible for developing Sciences and Engineering and has been the Head of the School of Mathematics, Computer Science and Engineering which he established at the University. He received a prestigious Commonwealth Fellowship for pursuing his doctorate (DPhil) in Applied Nonlinear Mathematics, which he earned from the University of York (UK) in 1996. He holds BSc (Hons), MSc, and MPhil (with distinction) in Mathematical Physics from the MDS University of Ajmer, India. Prior to joining Liverpool Hope, he was with the Brunel University, London. He is an internationally respected scholar working at the cutting edge of nonlinear mathematics, theoretical computer science, and systems engineering. He has edited volumes on Intelligent Systems, and Applied Mathematics. He is well published with over 450 publications in prestigious publishing outlets. He has an extensive background and experience of working in Universities in the UK and India. He has been an expert reviewer for the Biotechnology and Biological Sciences Research Council (BBSRC) grants peer-review committees for Bioinformatics Panel; Engineering and Physical Sciences Research Council (EPSRC) for High Performance Computing Panel; and served on the Peer-Review College of the Arts and Humanities Research Council (AHRC) as a scientific expert member. Prof Nagar sits on the JISC Research Strategy group and he is a fellow of the Institute of Mathematics and Its applications (FIMA) and a fellow of the Higher Education Academy (FHEA). **ORCID ID:** https://orcid.org/0000-0001-5549-6435.